# Bio-Inspired Ultrathin Piecewise Controllable Soft Robots

*Dengfeng Li, Song Wang, Jiahui He, Hao Zeng, Kuanming Yao, Zhan Gao, Mengge Wu, Yiming Liu, Lidai Wang, Zhaoqian Xie, Xinge Yu**

Dr. D. Li, S. Wang, J. He, K. Yao, Z. Gao, M. Wu, Y. Liu, Prof. L. Wang, Prof. X. Yu
Department of Biomedical Engineering
City University of Hong Kong
Hong Kong 999077, China

Dr. H. Zeng
Smart Photonic Materials, Faculty of Engineering and Natural Sciences
Tampere University
Tampere, Finland

Prof. Z. Xie
State Key Laboratory of Structural Analysis for Industrial Equipment, Department of Engineering Mechanics, International Research Center for Computational Mechanics
Dalian University of Technology
Dalian 116024, China.

Email: xingeyu@cityu.edu.hk

Keywords: Soft robotics, Bio-inspired electronics, Thermal actuators, Flexible electronics, Piecewise control

**Abstract**

In nature, animals or plants often use soft organs to move and hunt. Research works on bio-inspired materials and devices have attracted more and more interest as which show the potential for future intelligent robots. As key components of soft robots, biomimetic soft actuators are adapted to greater requirements for convenient, accurate, and programmable controlling robots. Here, we report a class of materials and processing routes of ultrathin actuators for bio-inspired piecewise controllable soft robots, where the actuators associate with thermal-responsible soft silicone thin film with thickness as thin as 45 μm and electrically driven by well mechanical designed metallic thin film electrodes. Multiple electrodes in the robots in charge of individual segments control allow the soft robots exhibiting similar functionalities of animals or plants (for example, imitating the tongue of a reptile, such as chameleon to hunt moving preys, and mimicking vines to tightly wind around objects). These bionics results in the soft robots demonstrate their advantages in precise and flexible operation, which provides a good reference for the future research of intelligent soft actuators and robots.

**Keywords:** Bio-inspired robots, Soft robots, Piecewise Control, Bi-layer film, Flexible electrode

## 1. Introduction

Intelligent robots are gradually playing crucial roles in the engineering and medical fields.(*1*)(*2*)(*3*)(*4*)(*5*) Inspired by natural creatures, bionics research on robots has attracted great of attentions as which could make robots more intelligent.(*6*) The trend of developing bio-inspired robots tends to be exploring materials and devices to act as "soft body" or "soft organs" in robots for realizing advanced mechanical attributes, great environmental adaptability and sophisticated applications. Through scientists' efforts from multidisciplinary fields, technologies in flexible electronics haven been proved to be a good foundation for future intelligent soft robots.(*7*)(*8*)(*9*)(*10*)(*11*) The intrinsic nature of "organs" in soft robots, such as hands, legs, tongue, etc. is various kinds of flexible actuators. Functional materials that can be responsible to electricity, temperature, magnetic field, and light, i.e. dielectric elastomer,(*12*) bilayer graphene(*13*)(*14*), thin magnetic membranes,(*15*) and liquid crystal elastomer (LCE),(*16*)(*17*) enable the corresponding flexible actuators generating obvious deformations to serve as the active organs in robots.(*18*) For instance, imitating animals' behaviors from insects' crawling and quadrupeds' walking allows scientists realizing insect-sized soft robots and three-dimensional (3D) robots with flexible limbs or body;(*19*)(*20*) mimicking the twining phenomena of the growing vines stimulates the development of screw-typed soft actuators.(*21*)(*22*)(*23*) The key point of developing these bionic soft robots is properly coordinating materials, structures and actuation modes.

To date, various actuation methods including magnetic field, light, heat, etc. have been adopted for driving soft actuators or robots.(*16*)(*24*)(*25*) Among these methods, magnetic field is one of the most used one, that associates with developing the main body of a robot by advanced manufacturing techniques, i.e. 3D or 4D printing to create programmed magnetization configuration that allows the robot deforming or moving under a unidirectional magnetic field.(*25*)(*26*) For actuators that respond to temperature or light, heat or light radiation can

converting thermal or optical energy to mechanical forces for deforming the structure of the actuator.(*27*)(*28*) Despite the progress of soft actuators based on the above mentioned actuation methods, the specific requirements such as external magnetic field controlling systems or accurate light sources are needed and thus significantly limit their applications.(*29*) Compare with these passive actuation methods, electrically control is an excellent active actuation method that shows many advantages in developing soft actuators.(*30*) On one hand, controllable and quantifiable electrical inputs allow precise controlling actuators to generate accurate and desired mechanical deformations without external heavy and complicated setups. On the other hand, electric based actuators also offer great compatibility of electronics integration with the control system in the robots. Thermal induced deformations in actuators by inputting electricity to conductive wires has been reported for soft actuators.(*24*) However, the dimension, especially the thickness of these soft actuators are still way too big, that limits their applications in biomedical areas.(*20*)(*31*) How to develop small size, ultrathin bio-inspired soft actuators raises to be one of the key problems in soft robots, and two specific tasks are need to be solved: *(1)* developing thin-film actuators with ultra-thin flexible electrodes; *(2)* endowing the biomimetic actuator ability of separated piecewise control to enhance its flexibility and controllability in various application scenarios.

In this work, we developed an ultrathin film that are responsible to thermal inputs for soft actuators by combining flexible electronic processing technologies and mechanics designs. A bi-layer thin film with significant difference of thermal expansion coefficient and a 200 nm-thick gold (Au) electrode was developed to serve as the actuator. The actuators exhibit a spiral shape with 900° bending in their original state, but can straighten out with electricity generated heat input through the electrode. To illustrate the advantages of the materials and mechanics in the soft actuators, we developed piecewise controllable soft robots based on these actuators by simply using multiple separated electrodes. These robots show great bionic capabilities, such

as mimicking the tongue of a chameleon to hunt a moving ant, and simulating a plant's vine to wind around a tiny pole. The precise programmed fabrication and piecewise control of the thin-film based soft actuators will provide important references for future bionic actuators and robots.

## 2. Materials and methods

### *2.1. Fabrication of thin-film actuator*

First, poly(methylmethacrylate) (PMMA) solution (20mg·mL$^{-1}$, chlorobenzene solvent) serving as a sacrificial layer was spin-coated on a quartz glass substrate and baked at 200 °C for 20 min. Afterward, poly(pyromellitic dianhydride-co-4,4'-oxydianiline), amic acid solution (Sigma-Aldrich) was spin-coated on the PMMA layer at 3000 rpm for 30 s and annealed at 250 °C for 30 min. The formed 2-μm polyimide (PI) film with low heat expansion coefficient was served as passive deformation layer. 200-nm Au was deposited onto the PI film by a sputtering system (Quorum Sputter coater, Q150 T S) and then coated by photoresist (AZ 5214) at 3000 rpm for 30 s with soft-bake of 110 °C for 3 min. After exposure under ultraviolent light with a film mask and development in AZ 300MIF developer, the Au layer was etched in the gold etchant ($I_2$/KI solution) to form the desired pattern. After removing the PMMA sacrificial layer in acetone for 12 hrs, the anisotropic conductive film (ACF) wire was connected with the acquired ultrathin gold electrode for further heating by external voltage source. Finally, the polydimethylsiloxane (PDMS, Sylgard 184, per-polymer and cross-link agent = 5:1) was spin-coated at 1000 rpm for 60 s on the electrode and cured at 75 °C for 30 min, serving as the positive deformation layer. After cutting and peeling the film off the substrate, the film was annealed on the hotplate at 150 °C for 10 min and cooled to room temperature in air to achieve a stable state. Thus, the helical actuator was acquired.

### *2.2. Actuation and characterization*

After bonding the ACF wire to a designed printed circuit board (PCB), the actuator was connected with a DC power source. When a certain voltage was applied, the actuator was heated

and straightened to present a state of elongation. All deformation processed were recorded with a macro-lens camera (SONY). Temperature changes of the heated actuators were recorded by an infrared camera (FLIR-C7200). The cross-section microstructure of the actuator was observed by using a scanning electron microscope (JEOL/JSM-5600). The thickness of actuators with different PDMS layers was measured by the optical surface profiler (OSP, Veeco/Wyko NT9300).

*2.3. Thermal simulation*

Electrothermal simulation is acquired based on the finite element analysis (FEA). The commercial software ABAQUS was used to study the temperature distribution of the one-electrode device with the heat convection coefficient (26 $W\ m^{-2}\ K^{-1}$) of air and an input power of 0.18 W. The entire device was modeled by hexahedron heat-transfer elements (DC3D8). Mesh convergence of the simulation was ensured for all the cases. The thermal conductivity, heat capacity and mass density used in the simulations were 315 $W \cdot m^{-1} \cdot K^{-1}$, 130 $J \cdot kg^{-1} \cdot K^{-1}$ and 19300 $kg \cdot m^{-3}$ for Au, 0.15 $W \cdot m^{-1} \cdot K^{-1}$, 1460 $J \cdot kg^{-1} \cdot K^{-1}$ and 965 $kg \cdot m^{-3}$ for PDMS, 0.12 $W \cdot m^{-1} \cdot K^{-1}$, 1090 $J \cdot kg^{-1} \cdot K^{-1}$ and 1420 $kg \cdot m^{-3}$ for PI.

## 3. Results and discussion

Figure 1a illustrates the schematic diagram of the ultrathin soft actuator and highlights the key materials used for it, consisting a 43 μm thick polydimethylsiloxane (PDMS) layer as the main body, a 200 nm thick Au electrode supported by a thin polyimide (PI, 2 μm thick) layer as thermal actuation part. Figure 1b shows the fabrication process of the soft actuator. The fabrication started on a clean glass substrate, where a thin poly(methylmethacrylate) (PMMA) layer was spin-coated and baked as the sacrificial layer. Then, poly(pyromellitic dianhydride-co-4,4’-oxydianiline), amic acid solution was spin-coated on the PMMA layer and annealed at 250 °C to form a 2 μm-thick dense PI film, as the passive deformation layer.(*32*) Next,

sputtering deposition and photo lithography defined 200 nm-thick Au thin layer on the PI layer formed the electro-thermal converting electrode.(*33*)(*34*) Immersing the sample in acetone for 12 hrs allowed fully dissolving PMMA and thus we could easily peel off the thin film from the glass substrate. After bonding ACF wire on the Au electrode pins, the heating electrode could be supplied by external power (Figure 1d). Finally, the PDMS with per-polymer and cross-link agent ratio of 5:1 was spin-coated on the PI and Au electrode at spinning speed of 1000 rpm for 60s and cured at 75 °C for 30 min. After cutting the edge of the sample into designed width of 4 mm, the actuator was peeled off with a straight shape (Figure 1c). In order to make the actuator own a stable steady state, an annealing process was carried out at 150 °C for 5 min. The high temperature annealing state made the PDMS layer being in excess of expansion, and thus resulted in a large shrinkage after cooling down to room temperature.(*35*)(*36*) Figures 1c and e present the state and shape of the actuator before and after annealing or actuation. The dynamic deformation process of the actuator on a hot plate at 150 °C can be seen in Movie S1. Thus, an ultrathin electrically controlled soft actuator with a helical structure is obtain. Cross-section scanning electron microscopy (SEM) image of the actuator shows clear thin layer structure, and the thickness of each layer was also measured and confirmed by an optical surface profiler to be 2 μm thick for PI and 43 μm thick for PDMS.

To study the effect of PDMS thickness on the actuator deformation ability, we prepared a group of soft actuators with different thick PDMS layers ranging from 43 μm to 178 μm by simply controlling the spinning durations at a fixed speed of 1000 rpm (Figures S1 and S2). The results showed that the deformation of PDMS is highly relevant with the thickness, where thicker layers induced the smaller deformations. As shown in Figure S1, the annealed 45 μm-thick actuator exhibits a 900° bending angle and the shortest length among all devices, demonstrating great performance of deformation and elongation during the actuating process. The heating area of the electrode is 2 mm in width and 32 mm in length (Figure S3). After

cutting into a 4 mm-wide stripe, the entire actuator could realize actual actuation on the 32 mm length, excluding the wire connection area. Figure 2a shows the original state and actuated state of the actuator under different voltage inputs, where we can find the actuator can fully straighten itself out under an voltage input of 10 V that equals to 179 mW since the resistance of the electrode is 558 Ω (Movie S2). The deformation process derives from the significant difference in thermal expansion coefficient between PI and PDMS. The thermal expansion coefficient of positive PDMS layer is around $310\times10^{-6}$ $K^{-1}$, that is more than 10 times greater than that of the passive PI layer with a value of $20\times10^{-6}$ $K^{-1}$.(*37*) Thermal energy generates greater expansion in the PDMS than that of PI layer, and thus causes the actuator to bend towards the PI layer (Figure 2a and 2b). The electrode in between PI and PDMS offers the actuators highly efficient thermal induced deformations compared to using external heat source such as a heat plate. Infrared (IR) camera recorded temperature information during the thermal actuating process provides quantitative data of the electric-thermal conversions, as shown in Figure 2d. The temperature reaches 62.3° under 10V voltage input, which is consistent with the finite element analysis (FEA) simulated results (Figure 2c). The actuator also exhibits good durability for long-term and multiple times operations, where the actuation capability still maintains the same after 100 cycles operation at 10 V (Figures 2e and S6). Since the actuation temperature did not exceed the annealing temperature of 150 °C, the heating would not cause changes of the material properties and the steady state of the structure. The maximum travel amplitude of the actuator is more than twice its initial body length of 14.5 mm to 32 mm, that lays a foundation for the various multi-functional bionic applications. Moreover, the actuator could elongate to different lengths in the range between 14.5 mm and 32 mm under controlled voltage inputs (Figure S4, Movie S2). The relationship between the elongate length and the voltage is summarized in Figure 2f, where we can find the relationship is stable and directed, which further reflects accuracy and precision of electrically control. Figures 2g and Figure S5 shows the great

linear behavior of actuation temperatures as a function of input voltage, which provides the basis for a specific control.

In addition, we also analyze the deformation process of the actuator during electrical heating and cooling in air. Figure S7 shows that it takes about 2 s to straighten out and 2.5 s to recover to the initial shape. During the straightening process, the actuator slowly elongates at the beginning but instantly straightens out in a short 0.2 s and then slowly turn to the final stable state. This phenomenon is due to an instantaneous release of the potential energy during the deformation process and thus cased a “hump” during the actuation process. This sudden and large deformation is quite similar to the predation behavior for a short time in the animal kingdom. In nature, many reptiles utilize their tongues to catch their preys. For example, geckos and chameleons crawling on the walls use their tongues to catch mosquitoes; anteaters feed on ants by sticking their long tongues into ants’ nests; frogs rely on their tongues to catch flies. Inspired by these hunting behaviors in nature, we used the soft actuator to mimic the chameleon’s tongue for hunting insects, as demonstrated in Figure 3. When a chameleon discovers a moving prey coming closer, it will stick out its tongue to capture the prey via the sticky part on the upper side of its tongue and then contract the tongue to bring the prey back to its mouth. Here, the soft actuator’s straightening and recovery process perfectly imitates the chameleon tongue during hunting process. So, we added a small amount of semi-cured PDMS on the top of the actuator to serve as the adhesive part of the tongue to the prey. Figure 3b shows the height of the ants during the hunting process, where “0” represents the ground height level. The hunting process can be divided into four parts: approaching, sticking, lifting and catching. As an ant walks nearby, the soft actuator is turned on by input electricity, heated and then stretched out to approach the ant. When the actuator is fully extended, it sticks to the ant’s body, and the entire actuation process is finished. Then, the turn-off of the electricity inputs allows the actuator starting to recovery process, and the ant is lifted up and can't escape from the

211 “tongue” because of sticky adhesion, which proves that the actuator can successfully and
212 accurately capture a moving insect. The entire capture process, shown in detail in Figure 3c and
213 Movie S3, is approximately 7 s while the instantaneous adhesion of the ant only takes less than
214 0.5 s. Benefiting from good flexibility and controllable deformation of the actuators, this work
215 provides a good example for the bionic animal tongue in the future.

216 In the plant kingdom, “soft actuators” on the plants’ body are still very common. Some
217 carnivorous plants, such as Venus flytrap and pitcher plants, are best known for controlling the
218 opening and closing of their organs to hunt preys. In addition, rattan plants around us also can
219 control the deformations of their whiskers or vines during growing. Rattan vines need to climb
220 or twine themselves around some branches. As the plant grows, it constantly looks for new
221 branches to twine around, making the whole body stronger. Interestingly, if another branch is
222 placed nearby, the well twined vine often opens part of its body and continue to twine around
223 the new branch, which reflects the wisdom of plant growth. Considering the same spiral shape
224 and deformable properties, we can also use our soft actuators or robot to mimic the plant's vines.
225 However, a single heating electrode can only control the deformation of the whole body with
226 one actuation mode, while in many cases, the robot with one actuator cannot be completely
227 twined around a branch by this simple actuation mode. Therefore, we introduced a double-
228 electrode system to realize piecewise independent control to make the soft robot more
229 intelligent (Figure 4a). The resistances of thermal actuator 1 and thermal actuator 2 are 275 Ω
230 and 304 Ω, respectively. As shown in Figure 4b, when the actuator 1 is on (5.5 V) and actuator
231 2 (5.5 V) is off, the root of the soft robot will straighten out, but the tip is still curved. Similarly,
232 when the actuator 1 is off and actuator 2 is on, the tip of the soft robot will straighten out, but
233 the boot is still curved (Movie S4). If both actuators are on and off at the same time, this soft
234 robot can be treated as a single-electrode version. The temperature distributions during the
235 piecewise control were also recorded, as shown in Figure 4d.

As shown in Figure 4e and Movie S5, a thin soldering wire is placed next to the soft robot to simulate a branch that plants twine around. When both actuator 1 and 2 are turned on, the device looks like a straight plant's vine. Firstly, we run the device in single-electrode mode that means turning off both electrodes at the same time, and the actuator gradually curls up into a spiral, trying to twine around the solder. At about 2 s, the root of the soft robot has been successfully twined. However, the top of the soft robot can't finish twining when it is fully recovered. The reason is that the top of the device recovers to spiral firstly, and the tip has already finished the deformation when the root begins to twine around the solder. To realize the successful performance as the true plant's behavior, the double-electrode mode is adopted. As demonstrated in Figure 4f, the end of the device is under the branch. After turning actuator 2 on, the tip of the device opens slowly. Then, when the actuator 2 is turned off again, the tip of the device begins to recover and place above the branch. Eventually, the soft robots successfully twined itself around the artificial branch. These results also provide ample evidences that electrically actuation can achieve pricewise control, regardless of the area of radiation that light or heat-driven actuators requires.(*29*)

This work provides only biomimetic examples of individual organs. In the future, depending on the principle of electronic control, more effective bionic actuators or robot could be achieved by introducing new thermal-response or electrical-response deformable materials and advanced structural or mechanical design.(*38*) In order to realize the real intelligent robots, complex intelligent feedback and control system is needed,(*39*) that requires the cooperation of more scientists in electrical engineering, computer science and control engineering.

## 4. Conclusion

In summary, we developed an ultrathin electrically controlled film for multifunctional bionic soft actuators. The 45 μm-thick actuator, containing passive invariant layer, nanoscale heating electrode and thermal expansion layer, exists in the initial state of a spiral structure.

Under different actuation voltages, unbending angle of the actuator can be precisely controlled. Moreover, after 100 cycles, the actuator's behavior is still completely repeatable. Given the similarities in structure and function, the actuators are used to imitate the chameleon's tongue and the vine of the plant. The artificial tongue can quickly straighten out and capture alive active ants. For plant biomimetic applications, the artificial vine with piecewise controllable double electrodes can be twined around a thin wire very easily. The introduction of double electrodes reflects the programmable and rich control ability of the electrical actuation, which will greatly promote the controllability and flexibility of soft robots. Meanwhile, this work also provides a good reference for the future development of bionic intelligent robot.

## Conflict of interest

The authors declare that they have no conflict of interest.


## Acknowledgements

This work was supported by City University of Hong Kong (Grants No. 9610423, 9667199), Research Grants Council of the Hong Kong Special Administrative Region (Grant No. 21210820), and Science and Technology of Sichuan Province (Grant No. 2020YFH0181).


## Author contributions

Dengfeng Li and Xinge Yu conceived the idea and designed the experiments. Xinge Yu supervised the project. Dengfeng Li, Song Wang, Jiahui He performed the experiments and characterizations. Zhaoqian Xie helped to perform the theoretical stimulation. All authors discussed the results and commented on the manuscript.

## Appendix A. Supplementary materials

Supplementary materials to this article can be found online at……

## References


1. B. Burger, P. M. Maffettone, V. V. Gusev, C. M. Aitchison, Y. Bai, X. Wang, X. Li, B. M. Alston, B. Li, R. Clowes, N. Rankin, B. Harris, R. S. Sprick, A. I. Cooper, A

mobile robotic chemist. *Nature*. **583**, 237–241 (2020).

2. J. W. Martin, B. Scaglioni, J. C. Norton, V. Subramanian, A. Arezzo, K. L. Obstein, P. Valdastri, Enabling the future of colonoscopy with intelligent and autonomous magnetic manipulation. *Nat. Mach. Intell.* **2**, 595–606 (2020).

3. A. Zemmar, A. M. Lozano, B. J. Nelson, The rise of robots in surgical environments during COVID-19. *Nat. Mach. Intell.* **2**, 566–572 (2020).

4. C. Wang, L. Dong, D. Peng, C. Pan, Tactile Sensors for Advanced Intelligent Systems. *Adv. Intell. Syst.* **1**, 1900090 (2019).

5. Z. Yuan, G. Shen, C. Pan, Z. L. Wang, Flexible sliding sensor for simultaneous monitoring deformation and displacement on a robotic hand/arm. *Nano Energy*. **73**, 104764 (2020).

6. A. Cully, J. Clune, D. Tarapore, J. B. Mouret, Robots that can adapt like animals. *Nature*. **521**, 503–507 (2015).

7. Y. Liu, R. Bao, J. Tao, J. Li, M. Dong, C. Pan, Recent progress in tactile sensors and their applications in intelligent systems. *Sci. Bull.* **65**, 70–88 (2020).

8. C. Wang, D. Peng, C. Pan, Mechanoluminescence materials for advanced artificial skin. *Sci. Bull.* **65**, 1147–1149 (2020).

9. X. Yu, Z. Xie, Y. Yu, J. Lee, A. Vazquez-guardado, H. Luan, J. Ruban, X. Ning, A. Akhtar, D. Li, B. Ji, Y. Liu, R. Sun, J. Cao, Q. Huo, Y. Zhong, C. Lee, S. Kim, P. Gutruf, C. Zhang, Y. Xue, Q. Guo, A. Chempakasseril, P. Tian, W. Lu, J. Jeong, Y. Yu, J. Cornman, C. Tan, B. Kim, K. Lee, X. Feng, Y. Huang, J. A. Rogers, Skin-integrated wireless haptic interfaces for virtual and augmented reality. *Nature*. **575**, 473–479 (2019).

10. B. Shih, D. Shah, J. Li, T. G. Thuruthel, Y.-L. Park, F. Iida, Z. Bao, R. Kramer-Bottiglio, M. T. Tolley, Electronic skins and machine learning for intelligent soft robots. *Sci. Robot.* **5**, eaaz9239 (2020).

11. L. Gu, S. Poddar, Y. Lin, Z. Long, D. Zhang, Q. Zhang, L. Shu, X. Qiu, M. Kam, A. Javey, Z. Fan, A biomimetic eye with a hemispherical perovskite nanowire array retina. *Nature*. **581**, 278–282 (2020).
12. T. Li, G. Li, Y. Liang, T. Cheng, J. Dai, X. Yang, B. Liu, Z. Zeng, Z. Huang, Y. Luo, T. Xie, W. Yang, Fast-moving soft electronic fish. *Sci. Adv.* **3**, e1602045 (2017).
13. Y. Yang, M. Zhang, D. Li, Y. Shen, Graphene-Based Light-Driven Soft Robot with Snake-Inspired Concertina and Serpentine Locomotion. *Adv. Mater. Technol.* **4**, 1800366 (2019).
14. Y. Dong, J. Wang, X. Guo, S. Yang, M. O. Ozen, P. Chen, X. Liu, W. Du, F. Xiao, U. Demirci, B. F. Liu, Multi-stimuli-responsive programmable biomimetic actuator. *Nat. Commun.* **10**, 4087 (2019).
15. X. Wang, G. Mao, J. Ge, M. Drack, G. S. Cañón Bermúdez, D. Wirthl, R. Illing, T. Kosub, L. Bischoff, C. Wang, J. Fassbender, M. Kaltenbrunner, D. Makarov, Untethered and ultrafast soft-bodied robots. *Commun. Mater.* **1**, 67 (2020).
16. H. Zeng, P. Wasylczyk, D. S. Wiersma, A. Priimagi, Light Robots: Bridging the Gap between Microrobotics and Photomechanics in Soft Materials. *Adv. Mater.* **30**, 1703554 (2018).
17. Y. C. Cheng, H. C. Lu, X. Lee, H. Zeng, A. Priimagi, Kirigami-Based Light-Induced Shape-Morphing and Locomotion. *Adv. Mater.* **32**, 1906233 (2020).
18. T. Yamaguchi, T. Kashiwagi, T. Arie, S. Akita, K. Takei, Human-Like Electronic Skin-Integrated Soft Robotic Hand. *Adv. Intell. Syst.* **1**, 1900018 (2019).
19. Y. Wu, J. K. Yim, J. Liang, Z. Shao, M. Qi, J. Zhong, Z. Luo, X. Yan, M. Zhang, X. Wang, R. S. Fearing, R. J. Full, L. Lin, Insect-scale fast moving and ultrarobust soft robot. *Sci. Robot.* **4**, eaax1594 (2019).
20. Q. He, Z. Wang, Y. Wang, A. Minori, M. T. Tolley, S. Cai, Electrically controlled liquid crystal elastomer-based soft tubular actuator with multimodal actuation. *Sci. Adv.*

**5**, eaax5746 (2019).

21. X. Pang, J. an Lv, C. Zhu, L. Qin, Y. Yu, Photodeformable Azobenzene-Containing Liquid Crystal Polymers and Soft Actuators. *Adv. Mater.* **31**, 1904224 (2019).

22. O. M. Wani, H. Zeng, A. Priimagi, A light-driven artificial flytrap. *Nat. Commun.* **8**, 15546 (2017).

23. D. Lunni, M. Cianchetti, C. Filippeschi, E. Sinibaldi, B. Mazzolai, Plant-Inspired Soft Bistable Structures Based on Hygroscopic Electrospun Nanofibers. *Adv. Mater. Interfaces.* **7**, 1901310 (2020).

24. M. Kanik, S. Orguc, G. Varnavides, J. Kim, Strain-programmable fiber-based artificial muscle. *Science*. **365**, 145–150 (2019).

25. Y. Kim, H. Yuk, R. Zhao, S. A. Chester, X. Zhao, Printing ferromagnetic domains for untethered fast-transforming soft materials. *Nature*. **558**, 274–279 (2018).

26. S. Wu, C. M. Hamel, Q. Ze, F. Yang, H. J. Qi, R. Zhao, Evolutionary Algorithm-Guided Voxel-Encoding Printing of Functional Hard-Magnetic Soft Active Materials. *Adv. Intell. Syst.* **2**, 2000060 (2020).

27. H. Zeng, H. Zhang, O. Ikkala, A. Priimagi, Associative Learning by Classical Conditioning in Liquid Crystal Network Actuators. *Matter*. **2**, 194–206 (2020).

28. T. H. Ware, M. E. McConney, J. J. Wie, V. P. Tondiglia, T. J. White, Voxelated liquid crystal elastomers. *Science*. **347**, 982–984 (2015).

29. M. Pilz da Cunha, S. Ambergen, M. G. Debije, E. F. G. A. Homburg, J. M. J. den Toonder, A. P. H. J. Schenning, A Soft Transporter Robot Fueled by Light. *Adv. Sci.* **7**, 1902842 (2020).

30. C. Wang, K. Sim, J. Chen, H. Kim, Z. Rao, Y. Li, W. Chen, J. Song, R. Verduzco, C. Yu, Soft Ultrathin Electronics Innervated Adaptive Fully Soft Robots. *Adv. Mater.* **30**, 1706695 (2018).

31. Y. Y. Xiao, Z. C. Jiang, X. Tong, Y. Zhao, Biomimetic Locomotion of Electrically

Powered “Janus” Soft Robots Using a Liquid Crystal Polymer. *Adv. Mater.* **31**, 1903452 (2019).

32. K. Yao, Y. Liu, D. Li, J. He, J. Li, R. H. W. Lam, Z. Xie, L. Wang, X. Yu, Mechanics designs-performance relationships in epidermal triboelectric nanogenerators. *Nano Energy*. **76**, 105017 (2020).

33. D. Li, C. Liu, Y. Yang, L. Wang, Y. Shen, Micro-rocket robot with all-optic actuating and tracking in blood. *Light Sci. Appl.* **9**, 84 (2020).

34. D. Li, Y. Liu, Y. Yang, Y. Shen, A fast and powerful swimming microrobot with a serrated tail enhanced propulsion interface. *Nanoscale*. **10**, 19673–19677 (2018).

35. S. Wang, Y. Gao, A. Wei, P. Xiao, Y. Liang, W. Lu, C. Chen, C. Zhang, G. Yang, H. Yao, T. Chen, Asymmetric elastoplasticity of stacked graphene assembly actualizes programmable untethered soft robotics. *Nat. Commun.* **11**, 4359 (2020).

36. Y. Ling, W. Pang, X. Li, S. Goswami, Z. Xu, D. Stroman, Y. Liu, Q. Fei, Y. Xu, G. Zhao, B. Sun, J. Xie, G. Huang, Y. Zhang, Z. Yan, Laser-Induced Graphene for Electrothermally Controlled, Mechanically Guided, 3D Assembly and Human–Soft Actuators Interaction. *Adv. Mater.* **32**, 1908475 (2020).

37. S. Yao, J. Cui, Z. Cui, Y. Zhu, Soft electrothermal actuators using silver nanowire heaters. *Nanoscale*. **9**, 3797–3805 (2017).

38. H. Cui, Q. Zhao, L. Zhang, X. Du, Intelligent Polymer-Based Bioinspired Actuators: From Monofunction to Multifunction. *Adv. Intell. Syst.*, 2000138 (2020).

39. X. Q. Wang, K. H. Chan, Y. Cheng, T. Ding, T. Li, S. Achavananthadith, S. Ahmet, J. S. Ho, G. W. Ho, Somatosensory, Light-Driven, Thin-Film Robots Capable of Integrated Perception and Motility. *Adv. Mater.* **32**, 2000351 (2020).

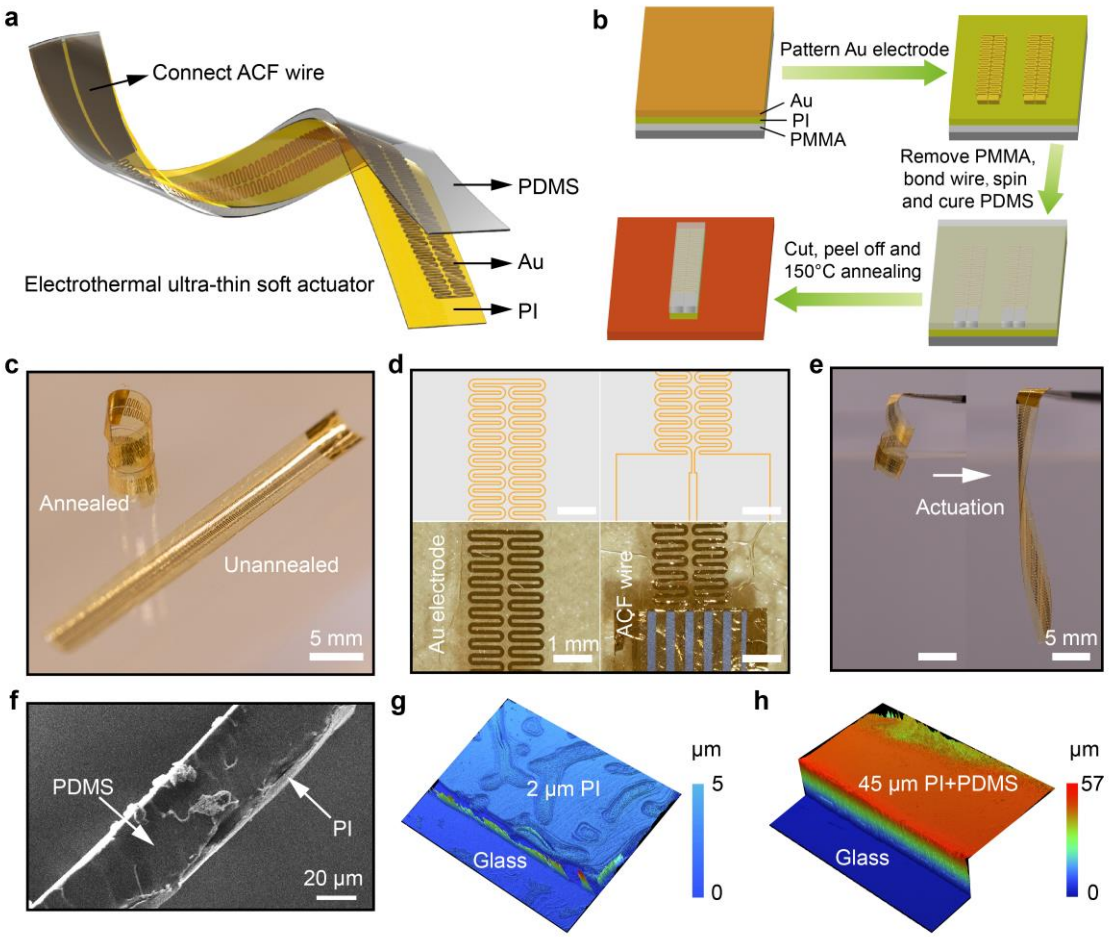


**Figure 1. Electrothermal ultra-thin soft actuator.** (a) Schematic diagram of the soft actuator. The thin film actuator consists an invariant PI layer, a 200 nm thick gold electrode, and a thermally expandable PDMS layer. (b) Flow chart of the fabrication process. Through lithography and wet etching for the patterned gold electrode, spin-coating of the flexible polymer PI and PDMS layers, the actuator is finally annealed to form a spiral structure. (c) Optical images of the annealed and unannealed film. (d) Structural design and optical images of the gold electrode, and the ACF wire connection for external voltage supply. (e) Optical images of a pensile actuator undergoing the annealing process. (f) Cross-section SEM images of the film. (g) Surface morphology and thickness of PI layer. (h) Surface morphology and thickness of film actuator.

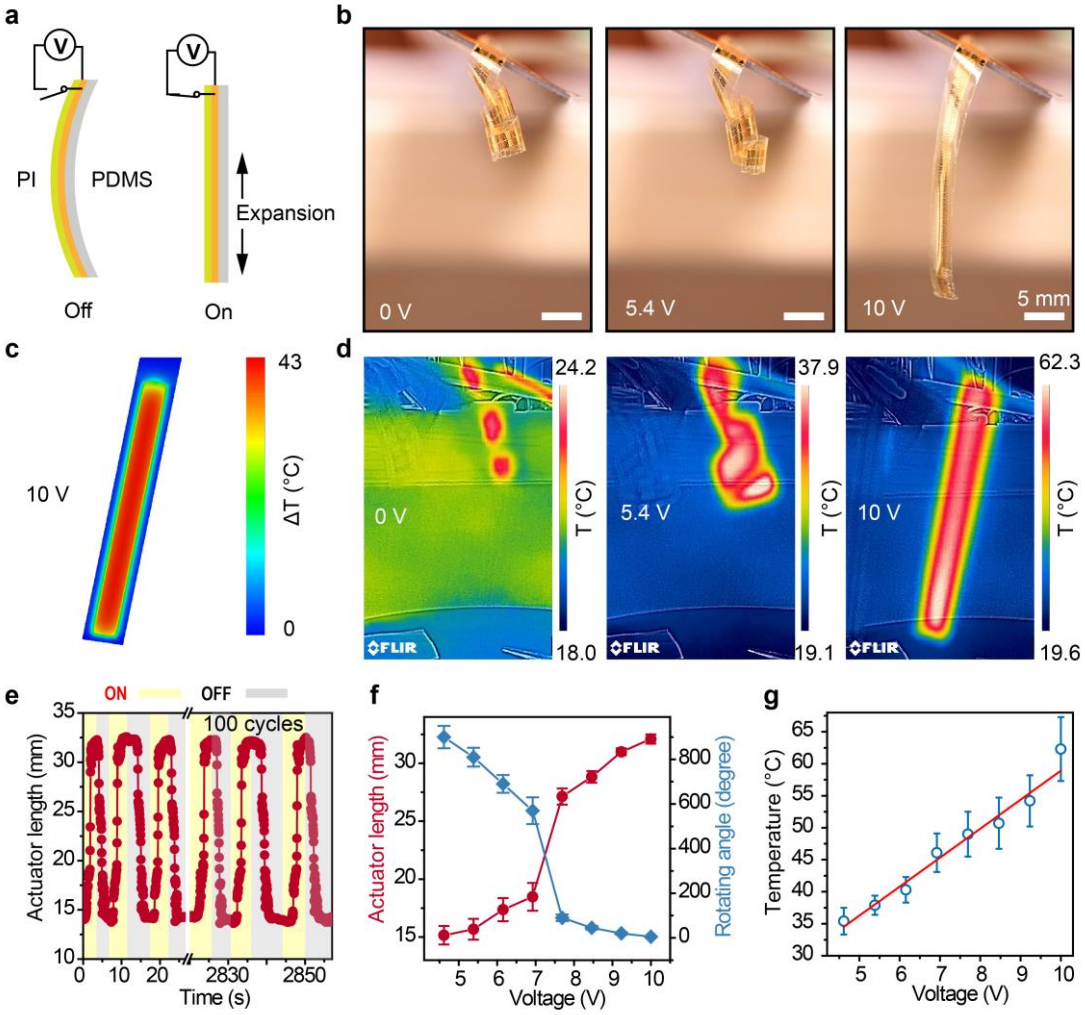


**Figure 2. Deformation performance under different actuating voltage.** (a) Schematic illustration of the actuating principle. (b) Optical images of actuator under different voltage inputs. (c) Temperature distribution in an actuator under 10 V simulated based on the finite element analysis (FEA). (d) IR camera recorded temperature distributions in the actuator under different voltage inputs. (e) Changes of actuator length during actuating and recovery for 100 cycles. (f) Relationships between actuator length/rotating angle and actuating voltages. (g) Relationship between the actuator temperature and actuating voltage.

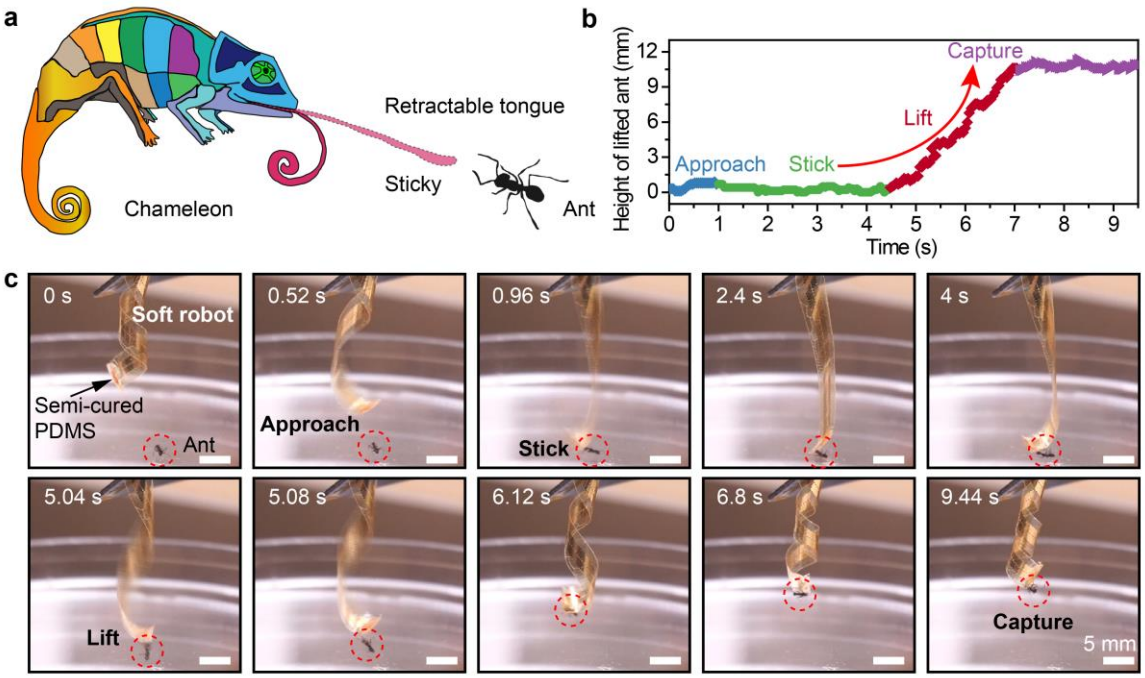


**Figure 3. Capturing an ant to mimic the tongue of a chameleon.** (a) Schematic illustration of a chameleon hunting process, where the tongue is straightening out to capture an ant. (b) The height of the ant prey varies with the hunting process: approaching, sticking, lifting and catching. (c)The hunting process of the artificial chameleon tongue. Semi-cured PDMS are used to mimic the viscosity of the tongue. The moving ant is successfully hunted within 10s.

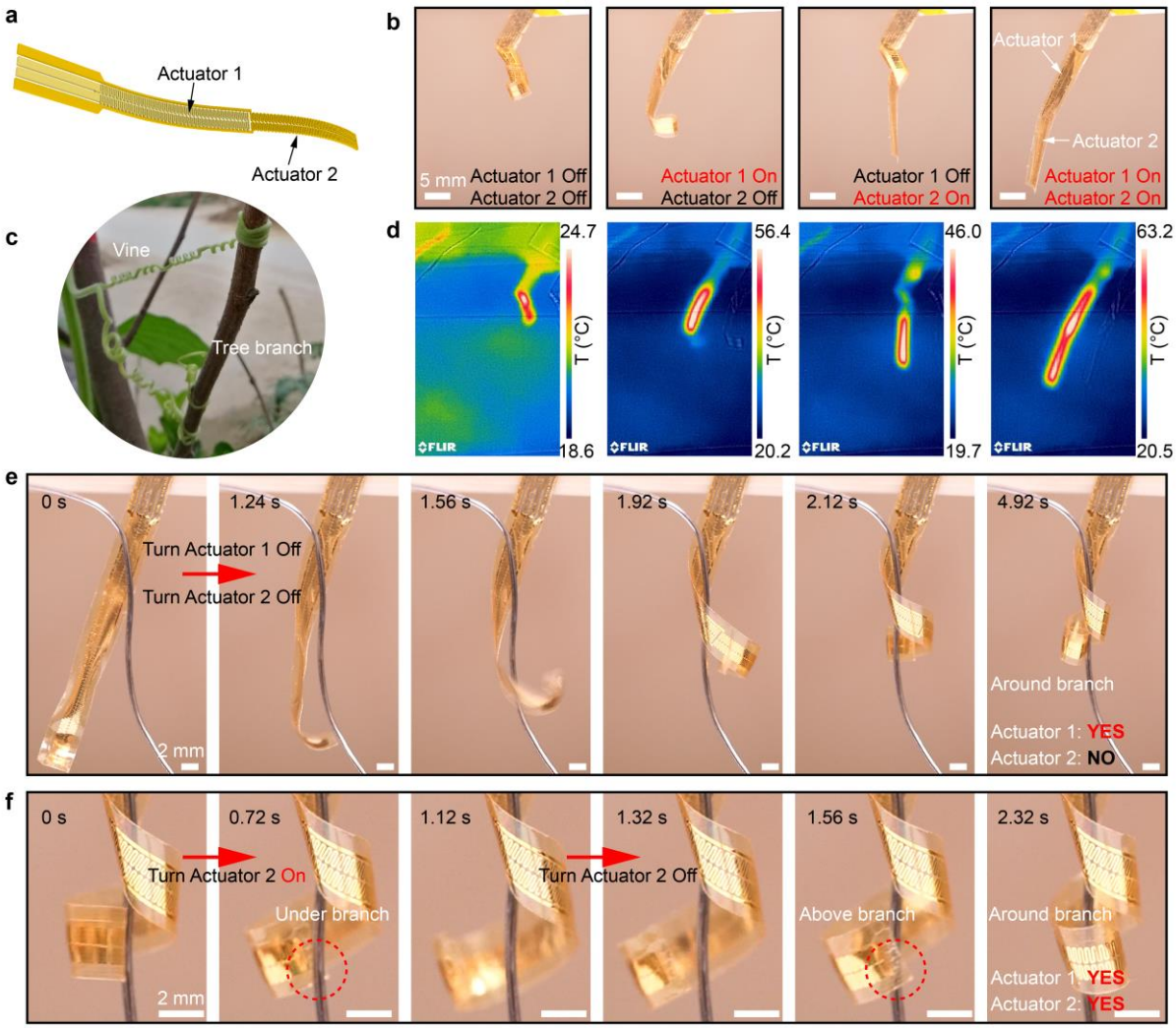


**Figure 4. Intelligent piecewise control of the soft robot for artificial vine.** (a) Design of the soft robot with double electrodes: actuator 1 and actuator 2. (b) Piecewise control by turning on each actuator separately. (c) A photo shows a vine of a gourd is twined around a tree branch. (d) Temperature distributions of the soft robot during piecewise control process. (e) Mimicking the twining process by the single-electrode mode that is turning on and off both actuators at the same time. (f) Achieving successful twining by piecewise control. Opening the top of the soft robot that fails to twine around the branch. The re-opening and closing allows the top to successfully twine around the branch as well.